Processing and Application of Ceramics 19 [3] (2025) 280–287
https://doi.org/10.2298/PAC2503280B

In situ Xe ion irradiation of Nd-doped $CaTiO_3$ perovskite ceramics to simulate nuclear waste immobilization

Nouar Bensemma[1,*], Ali Sari[1], Mir Anamul Haq[2], Dalila Moudir[3]

[1]*Nuclear Research Centre of Birine (CRNB), BP 180, Ain Oussera, Djelfa, Algeria*
[2]*MIAMI Irradiation Facility, School of Computing and Engineering, University of Huddersfield, UK*
[3]*Nuclear Research Center of Algiers (CRNA), 2 Bd Frantz Fanon, BP 399, RP-Algiers, Algeria*

Received 26 May 2025; Received in revised form 9 September 2025; Accepted 18 September 2025

Abstract

Developing efficient ceramic waste forms with high radiation stability for radioactive waste immobilization is very important for human and environmental safety. In this work, $Ca_{1-x}Nd_{2x/3}TiO_3$ (x = 0.225, 0.375 and 0.85) ceramics were prepared using solid state reaction method. Neodymium (Nd) was used as a surrogate for radioactive actinide species. The obtained ceramics have been characterized using XRD and Raman spectroscopy. To assess the performance of the ceramics in disposal conditions, heavy ion irradiation using 650 keV Xe with increasing doses was performed. The structural evolution of the irradiated compositions was monitored during ion irradiation using selected area electron diffraction (SAED). The results show that the radiation resistance is dependent on Nd concentrations, where the compositions with x = 0.225 and 0.375 exhibit the highest radiation stability. Furthermore, structure amorphization of the ceramics tends to increase with the increase of irradiation doses for all the compositions.

Keywords: *perovskites, nuclear applications, electron diffraction, amorphization*

I. Introduction

During the last four decades, nuclear energy has gained rapid development worldwide. This source of energy is used to satisfy increasing energy demands and considered to be a clean solution to global climate change. However, the main issue associated with nuclear industry is the radioactive waste generated during the nuclear energy production which causes radiation hazard to the bio-environment [1,2]. So, it has been an imperative to use sustainable and responsible pathways for the long-term safety and effective disposal of radioactive waste, especially high-level radioactive waste (HLW) such as long half-time minor actinides and fission products [3].

The immobilization of HLW requires the production of a solid, durable matrix containing the waste. Glass, glass-ceramics and ceramic waste forms are being considered as solid host matrices for HLW immobilization before deep geological disposal [4,5]. In the past few decades, various glass matrices had been widely employed for immobilization of high-level nuclear waste [6–8]. However, glass exhibits poor structural stability with low radiation tolerance and leaching resistance. In recent years, newer ceramic waste forms have been proposed to stabilize long-life minor actinides. Most results indicated that ceramic waste forms are more robust than glass matrices owing to their excellent chemical durability, thermodynamic and radiation stability [9–11].

Ceramic waste forms incorporating radioactive species have been used for safe long-term disposal into deep geological repositories [12,13]. During a long-term disposal, these matrices will be subjected to α-decay events from the incorporated radionuclides which result in accumulative atomic displacements. The induced radiation damage will ultimately deteriorate the physicochemical properties of the host ceramics [14,15]. Therefore, it is very important to investigate damage accumulation and amorphization process to evaluate long-term stability of the related ceramic waste forms.

Perovskite ABO_3 structure-type ceramics are widely used for long-term immobilization of radioactive cations such as trivalent actinides (Cm^{3+}, Am^{3+}, Pu^{3+})

*Corresponding author: +213 659275077
e-mail: *n.bensemma@crnb.dz*

and rare earth cations (Gd^{3+}, La^{3+}) [16]. The perovskite calcium titanate ($CaTiO_3$) ceramics was used as an immobilization matrix in the SYNROC solid solution [17]. It is designed to encapsulate radioactive strontium, trivalent actinides and lanthanides.

Radiation effect in perovskites is of interest due to their potential as actinide waste forms. Several experimental investigations have been previously performed to study the radiation-induced damage in perovskite ceramics. For example, Smith *et al.* [18] carried out extensive studies on the symmetry and structure changes of perovskite samples in the $La_xSr_{1-3x/2}TiO_3$ system under *in situ* 1.0 MeV Kr_2^+ irradiation. Lawson *et al.* [19] studied the radiation effect on $Ca_{1-x}La_{2x/3}TiO_3$ perovskites by using 1 MeV Kr and 5 eV Au ions. They pointed out the role of cation vacancies on the amorphization process. Lang *et al.* [20] carried out a study into the amorphization process in $CaZrO_3$ perovskite by using 940 MeV Au ions. Moreover, Whittle *et al.* [21] studied the role of vacancies on damage recovery in A-site deficient $Ca_{1-x}La_{2/3x}TiO_3$ perovskites using 1 MeV Kr ions.

However, controversial results of the radiation effects in deficient perovskites have been reported in the literature, especially the role of symmetry and cation vacancies on the radiation stability. Therefore, the purpose of the present study is to assess the radiation stability of a complex deficient $Ca_{1-x}Nd_{2x/3}TiO_3$ (x = 0.225, 0.375 and 0.85) perovskite type structure. In this study, we employed Nd^{3+} as a surrogate of trivalent actinides (An^{3+}) [22].

The objective of this study is to synthesize single phase deficient perovskite ceramics with the general formula $Ca_{1-x}Nd_{2x/3}TiO_3$ (x = 0.225, 0.375 and 0.85). The structural properties of the prepared samples were studied by XRD and Raman spectroscopy. To simulate the damage caused by α recoil nuclei in the ceramic waste forms, the samples were irradiated with 650 keV Xe. The amorphization of the samples as a function of the ceramics composition and irradiation doses has been investigated using selected area electron diffraction (SAED) with *in situ* ion irradiation.

II. Experimental

2.1. Samples preparation

$Ca_{1-x}Nd_{2x/3}TiO_3$ (x = 0.225, 0.375 and 0.85) ceramics were produced via conventional mixed oxide route. Stoichiometric amounts of starting raw materials of Nd_2O_3 ((≥99.0%, BIOCHIM, France), dried at 600 °C for 20 h, TiO_2 (>99.0%, BIOCHIM, France) and $CaCO_3$ (≥99.0%, BIOCHIM, France) were weighed and intimately ball-milled using a planetary mill (Pulverisette 5, FRITSCH Germany) with acetone to aid in mixing. As milling medium, zirconia vial (volume 80 ml) and balls made of same material (5 mm in diameter) were used. The mixture was milled for 3 h with 350 rpm. Afterwards the white suspension was sieved to separate it from the zirconia balls and dried in the compartment drier at 80 °C for 24 h. The fine mixture was calcined using a batch furnace CARBOLITE RHF1600 in air at 1300 °C for 20 h with a heating rate of 5 °C/min, then furnace cooled to room temperature. The calcined products were re-ground for 2 h at 350 rpm and re-calcined at 1300 °C for 20 h to obtain high purity samples. Subsequently, the powders were isostatically pressed into disc shaped samples with a diameter of 13 mm. Pressing is executed with 10 t/cm^2 and a duration of 5 min. Finally, the pellets were sintered in air at 1400 °C for 2 h at ramp of 3 °C/min, followed by natural cooling.

2.2. Characterization

The phase identification and structural analysis of all samples before irradiation were realized by room temperature X-ray diffraction (Philips PANalytical X'pert Pro diffractometer) with CuKα radiation (λ = 1.5406 Å). Diffraction patterns were recorded with a step of 0.026° from 10° to 100°. The HighScore software was used for phase identification through comparison of the diffraction patterns with the available Powder Diffraction File (JCPDS). Structural refinements were performed by the Rietveld method [23] using the FullProf program [24] which is integrated in WinPLOTR software package [25]. The structural model was built starting from the structural parameters of Sasaki *et al.* [26]. The pseudo-Voigt function was used to model the peak shape [27] with the cut-off value of 10.00× (full width at half maximum). The structural and profile factors such as: lattice parameters, scale factor, zero-shift error, background coefficients, peak profile, atomic positional parameters and isotropic (U_{iso}) atomic displacement parameters were simultaneously refined.

A LabRAM HR Evolution-Horiba instrument was used for Raman measurements. A calibration on a standard sample of silicon was carried out before each series of acquisitions. The ceramics $Ca_{1-x}Nd_{2x/3}TiO_3$ (x = 0.225, 0.375 and 0.85) were excited using a blue laser source with a well-defined wavelength of 473 nm. The spectra were recorded in the shift range from 100 to 1000 cm^{-1}. The spectrum obtained is the average of the 30 acquisitions.

2.3. Ion irradiations

Amorphization of the samples was studied using MIAMI TEM with an *in situ* ion irradiation facility at the University of Huddersfield in the United Kingdom. To obtain electron transparent samples, a small piece of the required sample (a few tens of milligrams) was ground in ethanol using a mortar and pestle and a drop of ethanol containing fine suspended particles was deposited on a TEM grid with a carbon film using a syringe needle. The samples were irradiated with 650 keV Xe ions using fluxes between 9.8×10^{11} and 1.3×10^{12} ions·cm^{-2}·s^{-1} and selected area electron diffraction (SAED) patterns were recorded at regular intervals to monitor the evolution of amorphization as a function of

time/fluence. In most cases, the experiments were repeated twice to obtain reliable amorphization fluence values. The electron beam was turned off during the ion irradiations to avoid any recrystallization induced by the electron beam and the TEM was operated at 300 keV.

III. Results and discussion

3.1. Structural characterization

XRD patterns of the $Ca_{1-x}Nd_{2x/3}TiO_3$ (x = 0.225, 0.375 and 0.85) samples are shown in Fig. 1. There are differences between the structures of the samples as a function of composition. The samples with x = 0.225, 0.375 were confirmed to have an orthorhombic *Pbnm* structure according to their successful indexation on the basis of perovskite $CaTiO_3$ phase (JCPDS 06-2149). The x = 0.85 sample has a perovskite monoclinic symmetry with space group $C2/m$. This symmetry is characterized by its main peaks corresponding to (001), (021), (022), (222), (400) and (242) planes in accordance with the structure reported previously by Lowndes *et al.* [28].

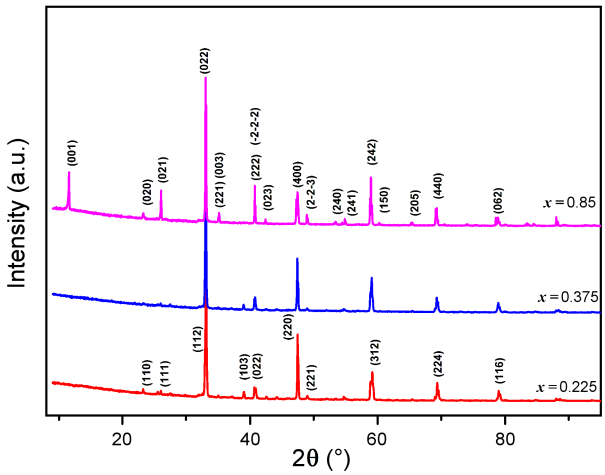

Figure 1. XRD patterns of $Ca_{1-x}Nd_{2x/3}TiO_3$ (x = 0.225, 0.75 and 0.85) ceramics

The Rietveld structure refinement of the $Ca_{1-x}Nd_{2x/3}TiO_3$ (x = 0.225 and 0.375) ceramics was done for the *Pbnm* space group while the structure of the composition x = 0.85 was refined from the monoclinic symmetry with space group $C2/m$.

Figure 2 shows the calculated, observed spectrum and their difference as well as the Bragg positions for the $Ca_{1-x}Nd_{2x/3}TiO_3$ (x = 0.225, 0.375 and 0.85) ceramics. The Rietveld refinements lead to good agreements between the experimental data and the theoretical models. Atomic positions and isotropic thermal agitation parameters of the $Ca_{1-x}Nd_{2x/3}TiO_3$ (x = 0.225, 0.375 and 0.85) ceramics as well as Rietveld refinement reliability factors are summarized in Tables 1 and 2, respectively.

Raman spectra of the $Ca_{1-x}Nd_{2x/3}TiO_3$ (x = 0.225, 0.375 and 0.85) ceramics recorded at room temperature are shown in Fig. 3. For the orthorhombic compositions with x = 0.225 and 0.375, there are 11 distinguishable

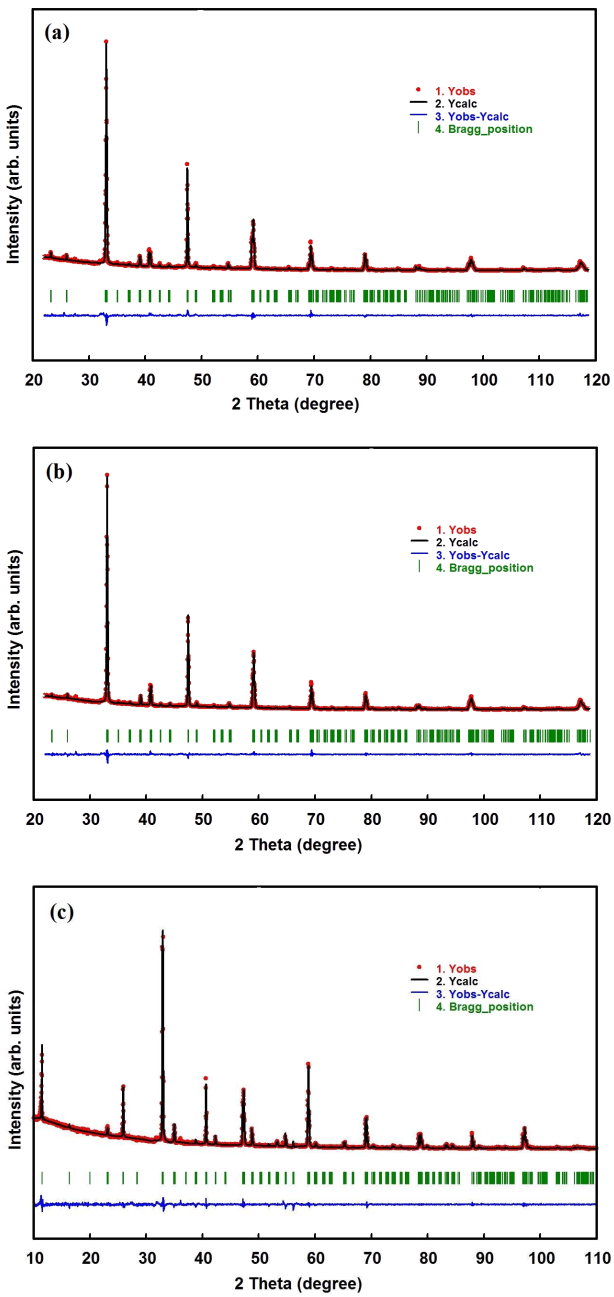

Figure 2. Profile fits for the Rietveld refinement of $Ca_{1-x}Nd_{2x/3}TiO_3$ ceramics: a) x = 0.225, b) x = 0.375 and c) x = 0.85

Raman bands in which their positions are close to those of $CaTiO_3$-materials found in several previous reports [29,30]. The bands located at 174, 208, 239, 287 and 340 cm^{-1} correspond to Ca–TiO_3 mode. The peaks located at 471 and 524 cm^{-1} are specific of torsional mode in the Ti–O_6 bonds, while the 650 cm^{-1} mode is due to the stretching of Ti–O bonds [29]. The band at 798 cm^{-1} corresponds to the symmetrical breathing of the oxygen [31]. Moreover, the mode observed at 130 cm^{-1} is attributed to the motion of A-site ions.

The monoclinic perovskite composition with x = 0.85 exhibits several bands located at 134, 247, 336, 460, 540 and 600 cm^{-1} which are in good agreement with

Table 1. Crystallographic data of the $Ca_{1-x}Nd_{2x/3}TiO_3$ (x = 0.225, 0.375 and 0.85) ceramics

	$Ca_{1-x}Nd_{2x/3}TiO_3$ (x = 0.225)	$Ca_{1-x}Nd_{2x/3}TiO_3$ (x = 0.375)	$Ca_{1-x}Nd_{2x/3}TiO_3$ (x = 0.85)
Symmetry	Orthorhombic	Orthorhombic	Monoclinic
Space group	*Pbnm* (No. 62)	*Pbnm* (No. 62)	$C2/m$ (No. 12)
Lattice parameters	a = 5.3969(1) Å	a = 5.4038 (3) Å	a =7.6806(2) Å
	b = 5.4395(1) Å	b = 5.4319 (2) Å	b = 7.6714(1) Å
	c = 7.6578(2) Å	c = 7.6576(1) Å	c = 7.7085(3) Å
			β = 90.016(1)°
Reliability factors			
R_B [%]	4.20	2.9	4.2
R_F [%]	4.60	3.20	5.3
R_{wp} [%]	14.8	14.6	16.1
R_p [%]	15.2	15.01	16.4
χ^2	1.50	1.53	1.95

Table 2. Atomic coordinates and isotropic thermal agitation parameters for $Ca_{1-x}Nd_{2x/3}TiO_3$ (x = 0.225, 0.375 and 0.85) ceramics

Atom	Site	x	y	Z	B (Å^2)
x = 0.225					
Ca/Nd	4c	0.99604(4)	0.03035(3)	0.25000	0.842(7)
Ti	4b	0.00000	0.50000	0.00000	0.471(6)
O1	4c	0.06677(3)	0.47615(6)	0.25000	0.540(5)
O2	8f	0.72411(4)	0.28656(5)	0.03721(3)	0.568(4)
x = 0.375					
Ca/Nd	4c	0.99440(12)	0.02540(09)	0.25000	0.990(8)
Ti	4b	0.00000	0.50000	0.00000	0.092(9)
O1	4c	0.06832(21)	0.48613(11)	0.25000	0.088(8)
O2	8f	0.71469(18)	0.28277(13)	0.03735(11)	0.703(6)
x = 0.85					
Ca1/Nd1	4i	0.253(9)	0.000	0.03000	0.324(7)
Ca2/Nd2	4i	0.252(3)	0.000	0.497(3)	0.951(8)
Ti	8j	-0.013(2)	0.253(2)	0.258(2)	0.325(3)
O1	4g	0.00	0.251(8)	0.00	0.452(3)
O2	4h	0.00	0.217(4)	0.050	0.246(3)
O3	4i	-0.035(2)	0.000	0.22(3)	0.321(2)
O4	4i	0.05(3)	0.500	0.269(7)	0.131(3)
O5	8j	0.230(5)	0.224(5)	0.209(7)	0.214(4)

those reported in the literature [32]. The Raman spectroscopy clearly indicates the structural transition from orthorhombic to monoclinic symmetry due to the overlapping of several bands and increase in the intensity of the mode at 134 cm^{-1} which reflects the increased A-site ions motion due to the high Nd doping level.

3.2. SRIM simulation

To predict experimentally produced damage and implant depth, Monte Carlo code SRIM 2013 was used to simulate the ion concentrations and the number of displacements per atom (dpa) as a function of irradiation depth. The simulations were performed in the "detailed calculation with full damage cascades" model.

Displacements per atom (dpa) of $Ca_{1-x}Nd_{2x/3}TiO_3$ (x = 0.225, 0.525 and 0.85) compositions were calculated by using the following formula [33]:

$$dpa = \left(\frac{vacancies}{ions \times \text{Å}}\right)\left(\frac{10^8(\frac{\text{Å}}{\text{cm}}) \times Fluence(\frac{ions}{\text{cm}^2})}{Atom\ density(\frac{atoms}{\text{cm}^3})}\right) \quad (1)$$

where damage-rate in ($vacancies/ions \times$ Å) is a computational file taken from the SRIM simulation outputs "vacancy.txt".

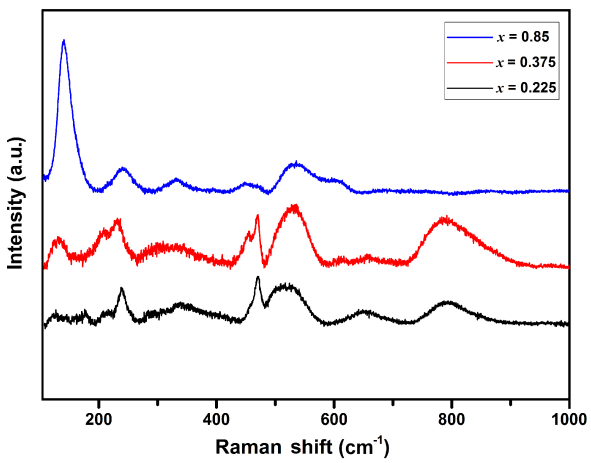

Figure 3. Raman spectra of $Ca_{1-x}Nd_{2x/3}TiO_3$ (x = 0.225, 0.75 and 0.85) ceramics

The calculated *dpa* and irradiation parameters for $Ca_{1-x}Nd_{2x/3}TiO_3$ (x = 0.225, 0.375 and 0.85) compositions are given in Table 3.

As an example, the damage profile obtained by SRIM simulation for the composition with x = 0.225 at different fluences is shown in Fig. 4. It can be seen that the damage peak is concentrated in the range of 0–300 nm for all the used fluences, so the accumulation of radiation damage is distributed in the shallow surface layer. We note that the induced damage increases with the increase of irradiation fluences and reaches its maximum at the highest fluence. The Xe ion implantation concentration gradually increases with depth, reaching a maximum value of 11 at.% at approximately 125 nm, as indicated in Fig. 4, before decreasing towards lower concentrations at greater depths. Consequently, this implantation profile suggests that Xe ions do not significantly affect the perovskite structure.

3.3. Amorphization studied by in situ ion irradiation

Amorphization was studied for the samples with x = 0.225, 0.375 and 0.85 at 295 K. The samples were considered fully amorphous when no diffraction spots were observed in the SAED patterns. Two amorphization experiments for each sample were carried out for x = 0.225 and 0.85 and the average of both is taken as the amorphization fluence. A single amorphization experiment was carried out for x = 0.375.

Zone axis [111] electron diffraction patterns for the $Ca_{1-x}Nd_{2x/3}TiO_3$ (x = 0.225, 0.375 and 0.85) ceramics are presented in Fig. 5. The transitions from crystalline-to-amorphous structure upon Xe ion irradiation were observed. For all samples, with increasing ion dose, the electron-diffraction maxima decrease in intensity until ultimately circular halo appears, characteristic of amorphous perovskite at the amorphization dose.

The crystalline-to-amorphous structure transition is the result of the accumulation of amorphous domains

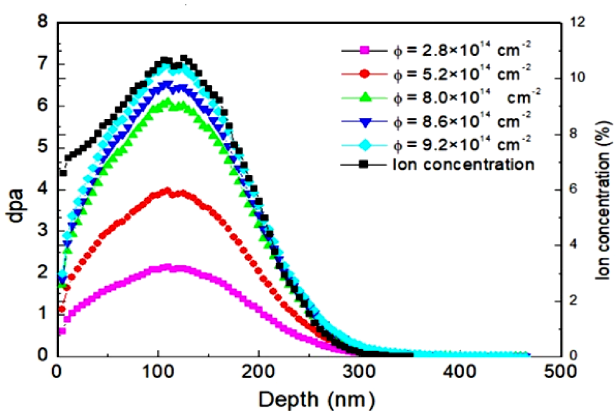

Figure 4. The damage profile calculated by SRIM obtained for the composition with x = 0.225

Table 3. The irradiation parameters and the *dpa* values of ceramic samples $Ca_{1-x}Nd_{2x/3}TiO_3$ (x = 0.225, 0.375 and 0.85)

Composition	Density [g/cm^3]	Irradiation Flux [ions/cm^2·s]	Irradiation fluences [ions/cm^2]	Irradiation doses [dpa]
x = 0.225	4.931	9.8×10^{11}	2.8×10^{14}	2.0123
			5.2×10^{14}	4.0041
			8.0×10^{14}	6.1617
			8.6×10^{14}	6.7212
			9.2×10^{14}	6.9890
x = 0.375	4.512	1.3×10^{12}	3.8×10^{13}	0.2534
			1.1×10^{14}	0.7512
			1.9×10^{14}	3.1824
			3.4×10^{14}	6.8024
			3.8×10^{14}	7.0857
x = 0.85	4.235	1.1×10^{12}	4.9×10^{12}	0.2139
			1.9×10^{13}	0.5240
			3.6×10^{13}	6.6033
			7.0×10^{13}	8.2451
			1.7×10^{14}	10.5126

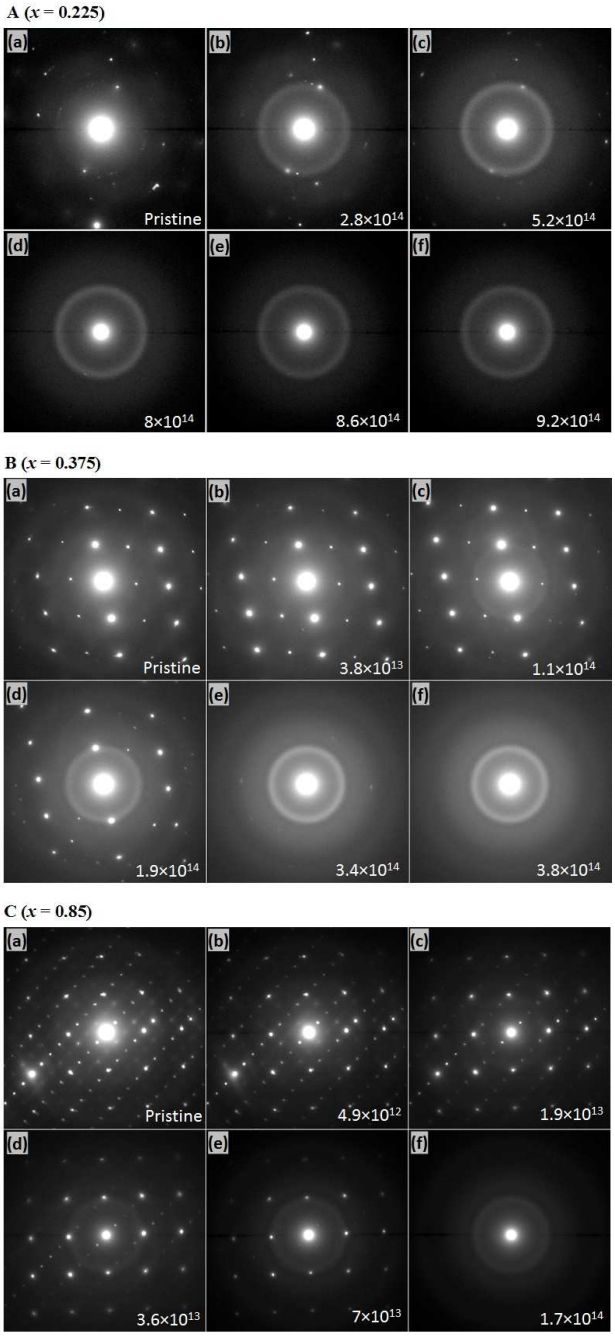

Figure 5. Changes of SAED patterns as a function of fluence for $Ca_{1-x}Nd_{2x/3}TiO_3$ ceramics: A) x = 0.225, B) x = 0.375 and C) x = 0.85

caused by ion-induced collision cascades. These cascades generate a high density of point defects and disordered regions; as the irradiation fluence increases, the overlap and interaction of these regions lead to a breakdown of the long-range crystalline order. When the defect density surpasses a critical threshold, the material undergoes amorphization. However, as shown in Fig. 6, the sample with the lowest Nd content (x = 0.225) has the greatest resistance to amorphization, and then there is a rapid drop as x increases from 0.225 to 0.375, after which there is only a slight drop in amorphization fluence. It is observed that as Nd doping level in-

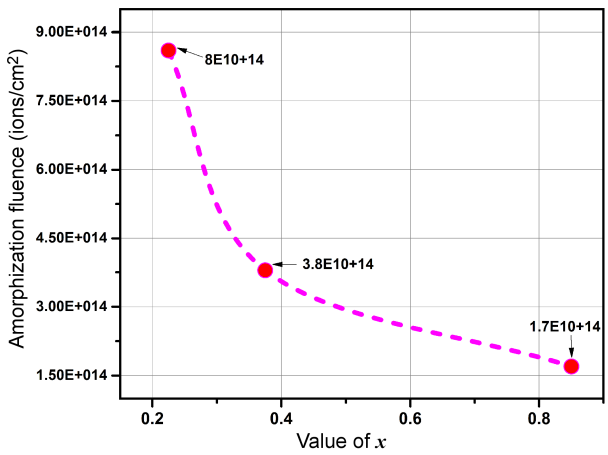

Figure 6. Amorphization fluences as a function of Nd doping level (x)

creases, the samples tend to amorphize at low ion irradiation fluence. This result can be explained by the increased rate of the induced vacancies. However, for our samples, the replacement of Ca^{2+} by Nd^{3+} ions in the perovskite A-site creates vacancies that tend to increase with the increase of Nd doping level and become more pronounced for the composition with x = 0.85. The transition from orthorhombic low Nd content phase (x = 0.225 and 0.375) to the monoclinic high Nd content phase (x = 0.85) leads to the creation of new lattice sites that can be occupied by the vacancies, leading to their redistribution and disordering. Compared to low Nd doping level compositions (x = 0.225 and 0.375), the disordered crystal lattice composition x = 0.85 exhibits high defect mobility under increased irradiation fluence which causes the amorphization to start from even low ion irradiation fluences.

Importantly, from a nuclear waste immobilization perspective, resistance to amorphization is a key criterion for the long-term stability of host matrices. Amorphization generally degrades the material's ability to retain radioactive ions by increasing their leachability. Therefore, materials that maintain crystallinity under irradiation are more suitable for immobilizing nuclear waste. In this context, the lower Nd-doped samples, particularly x = 0.225, show greater promise due to their higher radiation tolerance.

IV. Conclusions

To simulate the radiation effects in ceramic waste form under disposal conditions, the behaviour under *in situ* Xe ion irradiation of $Ca_{1-x}Nd_{2x/3}TiO_3$ (x = 0.225, 0.375 and 0.85) perovskite ceramics was studied in this paper. The ceramic pellets were prepared by using solid-state reaction method. Structural Rietveld refinements revealed that the compositions with x = 0.225 and 0.375 adopt an orthorhombic symmetry with *Pbmn* space group. With the rise of Nd doping level (x = 0.85), a phase transition to a monoclinic symmetry with space group $C2/m$ was identified. From Raman spectroscopy

results, the presence of eleven Raman active vibrational modes were confirmed for the compositions with x = 0.225 and 0.375 while six vibrational modes were identified for the composition with x = 0.85. The Raman results indicate the phase transition from orthorhombic to monoclinic symmetry in agreement with the Rietveld structural refinement results. To monitor the evolution of amorphization process, samples were irradiated with 650 keV Xe ions using increasing irradiation doses. The selected area electron diffraction (SAED) patterns were recorded *in situ* during irradiation. It was found that the sample with x = 0.225 has the greatest resistance to amorphization reflected by the highest fluence of amorphization. On the other hand, a remarkable drop in amorphization fluence was observed for the monoclinic phase with x = 0.85 which is explained by the increased rate of the induced vacancies due to the change in symmetry. From this study, it can be concluded that the explored Nd-doped $CaTiO_3$ perovskite ceramics with the compositions x = 0.225 and 0.375 possess enhanced structural stability under increased irradiation doses, which is suitable for disposal conditions.

Acknowledgement: This work is undertaken under the INWARD coordinated research project (Ion Beam Irradiation for High Level Nuclear Waste Form Development, F11022) which is a collaborative research on the subject supported by the IAEA (International Atomic Energy Agency).

References

1. W.J. Weber, A. Navrotsky, S. Stefanovsky, E.R. Vance, E. Vernaz, "Materials science of high-level nuclear waste immobilization", *MRS Bull*., **34** [1] (2009) 46–53.
2. N. Clavier, R. Podor, N. Dacheux, "Crystal chemistry of the monazite structure", *J. Eur. Ceram. Soc*., **31** [6] (2011) 941–976.
3. M.I. Ojovan, S.V. Yudintsev, "Glass, ceramic, and glass-crystalline matrices for HLW immobilization", *Open Ceram.*, **14** (2023) 100355.
4. I.W. Donald, B. Metcalfe, R.J. Taylor, "The immobilization of high level radioactive wastes using ceramics and glasses", *J. Mater. Sci*., **32** [22] (1997) 5851–5887.
5. P. Sengupta, "A review on immobilization of phosphate containing high level nuclear wastes within glass matrix - Present status and future challenges", *J. Hazard. Mater*., **235-236** (2012) 17–28.
6. V.S. Thorat, R.K. Mishra, V. Sudarsan, A. Kumar, A.K. Tyagi, C.P. Kaushik, "Leaching studies on borosilicate glasses for the immobilization of high-level radioactive waste in the pellet form subjected to aggressive test conditions", *Bull. Mater. Sci*., **42** (2019) 211–218.
7. C. Lopez, X. Deschanels, J.M. Bart, J.M. Boubals, C.D. Auwer, E. Simon, "Solubility of actinide surrogates in nuclear glasses", *J. Nucl. Mater*., **312** (2003) 76–80.
8. A. Brehault, D. Patil, H. Kamat, R.E. Youngman, L.M. Thirion, J.C. Mauro, C.L. Corkhill, J.S.M. Cloy, A. Goel, "Compositional dependence of solubility/retention of molybdenum oxides in aluminoborosilicate-based model nuclear waste glasses", *J. Phys. Chem. B*, **122** (2018) 1714–1729.
9. S.V. Stefanovsky, S.V. Yudintsev, "Titanates, zirconates, aluminates and ferrites as waste forms for actinide immobilization", *Russ. Chem. Rev*., **85** [9] (2016) 962–994.
10. A.E. Ringwood, P.M. Kelly, "Immobilization of high-level waste in ceramic waste forms", *Phil. Tram. R. Soc. Land. A*, **319** (1986) 63–82.
11. J. Ma, Z. Fang, X. Yang, B. Wang, F. Luo, X. Zhao, X. Wang, Y. Yang, "Investigating hollandite–perovskite composite ceramics as a potential waste form for immobilization of radioactive cesium and strontium", *J. Mater. Sci*., **56** (2021) 9644–9654.
12. L. Wang, T. Liang, "Ceramics for high level radioactive waste solidification", *J. Adv. Ceram*., **1** [3] (2012) 194–203.
13. M. Jafara, S.B. Phapalea, B.P. Mandala, M. Roya, S.N. Acharya, R. Mishraa, A.K. Tyagi, "Effect of temperature on phase evolution in $Gd_2Zr_2O_7$: A potential matrix for nuclear waste immobilization", *J. Alloys Compd*., **867** (2021) 159032.
14. Y. Ding, Z. Jiang, Y. Li, H. Dan, X. Lu, Y. Yang, T. Duan, "Effect of alpha-particles irradiation on the phase evolution and chemical stability of Nd-doped zircon ceramics", *J. Alloys Compd*., **729** (2017) 483–491.
15. C. Tamain, A. Özgümüs, N. Dacheux, F. Garrido, L. Thomé, "Effects of irradiation on the thorium phosphate diphosphate ceramics and consequences on its dissolution", *J. Nucl. Mater*., **352** (2006) 217–223.
16. A.E. Ringwood, V.M. Oversby, S.E. Kesson, N.G. Ware, W. Hibberson, A. Major, "Immobilization of high-level nuclear reactor wastes in SYNROC: A current appraisal", *Nucl. Chem. Waste Manage*., **2** (1981) 287–305.
17. K.L. Smith, G.R. Lumpkin, M.G. Blackford, R.A. Day, K.P. Hart, "The durability of Synroc", *J. Nucl. Mater*., **190** (1992) 287–294.
18. K.L. Smith, G.R. Lumpkin, M.G. Blackford, M. Colella, N.J. Zaluzec, "In situ radiation damage studies of $La_xSr_{1-3x/2}TiO_3$ perovskites", *J. Appl. Phys*., **103** (2008) 083531.
19. S.M. Lawson, N.C. Hyatt, R.K.L. Whittle, A.S. Gandy, "Resistance to amorphisation in $Ca_{1-x}La_{2x/3}TiO_3$ perovskites – A bulk ion-irradiation study", *Acta Mater*., **180** (2019) 180–188.
20. M. Lang, F. Zhang, W. Li, D. Severin, M. Bender, S. Klaumünzer, C. Trautmann, R.C. Ewing, "Swift heavy ion-induced amorphization of $CaZrO_3$ perovskite", *Nucl. Instrum. Methods Phys. Res. B*, **286** (2012) 271–276.
21. K.R. Whittle, M. de los Reyes, R.D. Aughterson, M.G. Blackford, K.L. Smith, P. Baldo, E.P. Ryan, N.J. Zaluzec, G.R. Lumpkin, "In-situ irradiation of $Ca_{1-x}La_{2/3x}TiO_3$ defect perovskites: The role of vacancies in recovery", *Materialia*, **3** (2018) 186–191.
22. G.T. Seabrug, "Overview of the actinide and lanthanide (the f) elements", *Radiochim. Acta*, **61** (1993) 115–122.
23. H.M. Rietveld, "Line profiles of neutron powder-diffraction peaks for structure refinement", *Acta Crystallogr*., **22** (1967) 151–152.
24. J. Rodríguez-Carvajal, "Recent advances in magnetic structure determination by neutron powder diffraction", *Phys. B Phys. Condens. Matter*., **192** (1993) 55–69.
25. T. Roisnel, J. Rodríguez-Carvajal, "WinPLOTR: A windows tool for powder diffraction pattern analysis", *Mater.*

Sci. Forum, **378-381** (2001) 118–123.
26. S. Sasaki, C.T. Prewitt, J.D. Bass, "Orthorhombic perovskite $CaTiO_3$ and $CdTiO_3$: structure and space group", *Acta Crystallogr. C*, **43** (1987) 1668–1674.
27. H. Toraya, "Array-type universal profile function for powder pattern fitting", *J. Appl. Crystallogr.*, **23** (1990) 485–491.
28. R. Lowndes, F. Azough, R. Cernik, R. Freer, "Structures and microwave dielectric properties of $Ca_{(1-x)}Nd_{2x/3}TiO_3$ ceramics", *J. Eur. Ceram. Soc.*, **32** (2012) 3791–3799.
29. U. Balachandran, N.G. Eror, "Laser-induced Raman scattering in calcium titanate", *Solid. State. Commun.*, **44** (1982) 815–818.
30. J. Fan, K. Du, Z.Y.Zou, C. Z.Yin, Y. B.Guo, F. Wang, Q. Zhao, X. H.Wang, W.Z. Lu, W. Lei, "Impedance spectroscopy, B-site cation ordering and structure-property relations of $(1-x)La[Al_{0.9}(Mg_{0.5}Ti_{0.5})_{0.1}]O_3$–$xCaTiO_3$ ceramics for 5G dielectric waveguide filters", *Ceram. Int.*, **47** (2021) 15319–15327.
31. J. Goethals, A. Bedidi, C. Fourdrin, M. Tarrida, S. Rossano, "Experimental study of trivalent rare-earth element incorporation in $CaTiO_3$ perovskite: evidence for a new substitution mechanism", *Phys. Chem. Miner.*, **46** (2019) 1003–1015.
32. R. Lowndes, M. Deluca, F. Azough, R. Freer, "Probing structural changes in $Ca_{(1-x)}Nd_{2x/3}TiO_3$ ceramics by Raman spectroscopy", *J. Appl. Phys.*, **113** (2013) 044115.
33. A. Dutta, K. Das, N. Gayathri, R. Menon, P.Y. Nabhiraj, P. Mukherjee, "Effect of Ar^{9+} irradiation on Zr-1Nb-1Sn-0.1Fe alloy characterized by grazing incidence X-ray diffraction technique", *Radiat. Phys. Chem.*, **144** (2018) 125–131.